AIAA 98-2444

Aerodynamic Computations Using The Convective Upstream Split Pressure Scheme With Local Preconditioning

M. Nemec and D. W. Zingg
Institute for Aerospace Studies
University of Toronto
Toronto, Ontario, Canada

29th AIAA Fluid Dynamics Conference
June 15-18, 1998/Albuquerque, NM

Aerodynamic Computations Using The Convective Upstream Split Pressure Scheme With Local Preconditioning

M. Nemec* and D. W. Zingg†
Institute for Aerospace Studies
University of Toronto
Toronto, Ontario, Canada

The implementation of the convective upstream split pressure (CUSP) approach to numerical dissipation is presented for an approximately-factored algorithm in conjunction with time-derivative local preconditioning. An inexpensive flux limiter is used to blend the low and high-order CUSP dissipation in order to enforce monotonic solutions. The resulting algorithm is applied to several turbulent aerodynamic flows and compared with results computed using the matrix dissipation scheme. The results show the CUSP scheme to be very effective in providing good shock capturing, low numerical dissipation in boundary layers, and low numerical errors. Accuracy is not compromised when the limiter is based on the pressure variable only, leading to significant savings in computational expense. For freestream Mach numbers below 0.2, the convergence rate and accuracy of the solver are significantly improved by preconditioning the CUSP scheme. Overall, the CUSP scheme is highly competitive with matrix dissipation in terms of accuracy at a reduced cost.

Introduction

NUMERICAL dissipation is a necessary evil in computations of aerodynamic flows. That is, the difference approximation for the convective fluxes cannot be purely skew-symmetric. The purpose of the symmetric, or dissipative, component of the difference approximation is to produce stable oscillation-free solutions without significantly compromising solution accuracy, while minimizing the cost of the algorithm. A numerical dissipation scheme has three components:

- A basic symmetric operator applicable to scalar flux functions.
- A flux splitting which ensures that all waves are appropriately dissipated when the above operator is applied to a hyperbolic system of equations.
- Some sort of flux limiting or switch in order to avoid oscillations near shock waves and other discontinuities without contaminating the solution in smooth regions of the flow.

The strategies chosen for each of these components can greatly influence the effectiveness and cost of the scheme.

During the early 1980s, the most popular numerical dissipation scheme in aerodynamic computations was the scalar scheme of Jameson *et al.*[1] (referred to as the JST scheme), with a simple pressure switch for shock detection. With this scheme, each wave receives dissipation corresponding to the maximum eigenvalue of the inviscid flux Jacobian. The scalar scheme is inexpensive and robust, but tends to be excessively dissipative in boundary layers.[2,3] Later in the decade, more sophisticated schemes gained in popularity, primarily as a result of their improved discontinuity capturing capabilities. These include flux-difference split upwind schemes[4,5] and the matrix dissipation scheme,[6] possibly combined with flux limiters based on TVD concepts.[7] Such schemes, often called high-resolution schemes, are more expensive per grid node than the JST scheme but are usually more cost effective as a result of their improved accuracy.

More recently, Jameson[8,9] introduced the convective upstream split pressure (CUSP) scheme, with the goal of providing the accuracy of a high-resolution scheme with a cost comparable to the JST scheme. There are two versions, HCUSP, which enforces a constant stagnation enthalpy and would appear to be more applicable to steady inviscid flows, and ECUSP. Preliminary results presented by Tatsumi *et al.*[10] were very encouraging. However, Swanson *et al.*[11] performed an evaluation of the HCUSP scheme and found it to be somewhat less accurate than matrix dissipation and up to 25% more expensive than matrix dissipation with a simple pressure switch.

*Graduate Student, marian@oddjob.utias.utoronto.ca.
†Associate Professor, Member AIAA.

In this paper, we present a thorough evaluation of the ECUSP scheme in the context of two-dimensional turbulent flow over airfoils. We examine dissipation levels in boundary layers, shock-capturing capability, global solution errors, convergence rates, and cost. A number of different flux limiting options are compared as well. It has been demonstrated by various researchers that the accuracy of a numerical dissipation scheme at low Mach numbers can be improved through the use of local preconditioning.[12] Hence we also present a locally preconditioned version of the CUSP scheme using the preconditioner of Weiss and Smith.[13]

Governing Equations and Numerical Method

The matrix and CUSP numerical dissipation schemes have been implemented in the thin-layer Navier-Stokes solver ARC2D.[14] This solver uses second-order centered differences in space through a generalized curvilinear coordinate transformation and is thus applicable to structured grids. Convergence to steady state is achieved using the diagonal form of the Beam and Warming approximate-factorization algorithm with local time stepping. The effects of turbulence are modeled by the Baldwin-Lomax turbulence model. A circulation correction is used at the outer boundary.

In two-dimensional generalized coordinates, the thin-layer Navier-Stokes equations are given by[14]

$$\frac{\partial \widehat{Q}}{\partial t}+\frac{\partial \widehat{E}}{\partial \xi}+\frac{\partial \widehat{F}}{\partial \eta}=\mathrm{Re}^{-1}\frac{\partial \widehat{S}}{\partial \eta} \tag{1}$$

where $\widehat{Q}=J^{-1}Q=J^{-1}[\rho,\rho u,\rho v,e]^T$ is the vector of conservative dependent variables, $\widehat{E}$ and $\widehat{F}$ are the convective flux vectors, $\widehat{S}$ is the viscous flux vector, ξ and η are the streamwise and normal generalized coordinates, respectively, J is the Jacobian of the coordinate transformation, and Re is the freestream Reynolds number based on the speed of sound.

The implementation of local preconditioning into the ARC2D solver is described by Unrau and Zingg,[12] and is based on the work of Weiss and Smith,[13] Choi and Merkle,[15] and Turkel.[16] The preconditioning technique not only accelerates the convergence rate of the solver, but also improves the accuracy of the solution for low Mach number flow. The preconditioned form of Eq. 1 is obtained by introducing the preconditioning matrix Γ as follows

$$\Gamma\frac{\partial \widehat{Q}}{\partial t}+\frac{\partial \widehat{E}}{\partial \xi}+\frac{\partial \widehat{F}}{\partial \eta}=\mathrm{Re}^{-1}\frac{\partial \widehat{S}}{\partial \eta} \tag{2}$$

In order to simplify the form of the preconditioning matrix, the following symmetry variables are used[12]

$$\partial\tilde{Q}=J^{-1}\left[\begin{array}{c}\frac{1}{\rho c}\partial p\\ \partial u\\ \partial v\\ \partial p-c^2\partial\rho\end{array}\right] \tag{3}$$

The symmetry variables are related to the conservative variables through the transfer matrices given by,

$$M=\frac{\partial\widehat{Q}}{\partial\tilde{Q}},\ M^{-1}=\frac{\partial\tilde{Q}}{\partial\widehat{Q}} \tag{4}$$

The local preconditioner formulated in terms of the symmetry variables can be applied to the thin-layer Navier-Stokes equations written in terms of the conservative variables as follows[12]

$$M\tilde{\Gamma}M^{-1}\frac{\partial \widehat{Q}}{\partial t}+\frac{\partial \widehat{E}}{\partial \xi}+\frac{\partial \widehat{F}}{\partial \eta}=\mathrm{Re}^{-1}\frac{\partial \widehat{S}}{\partial \eta} \tag{5}$$

The preconditioner of Weiss and Smith,[13] written in terms of the symmetry variable, has the following form

$$\tilde{\Gamma}=\left[\begin{array}{cccc}\frac{1}{\epsilon}&0&0&0\\0&1&0&0\\0&0&1&0\\0&0&0&1\end{array}\right] \tag{6}$$

where

$$\epsilon=\min\left[1,\max\left(\mathrm{M}^2,\epsilon_1\right)\right] \tag{7}$$

The parameter ϵ_1 is used to ensure that ϵ remains finite in stagnation regions and is given by

$$\epsilon_1=\phi\mathrm{M}_\infty^2 \tag{8}$$

where $\phi=1$ for the presented test cases.

Numerical Dissipation Schemes

Matrix Dissipation with Pressure Switch

Since the matrix numerical dissipation scheme is used for comparison purposes to evaluate the CUSP scheme, we present our implementation here. The matrix scheme is based on that of Swanson and Turkel,[6] and is added to the second-order centered difference scheme in generalized coordinates in the following manner:

$$\frac{\partial\widehat{E}}{\partial\xi}\approx\delta_\xi\widehat{E}-\nabla_\xi D_1 D_2 \tag{9}$$

with

$$\begin{aligned}
D_1 &= |A|_{j+\frac{1}{2},k}J^{-1}_{j+\frac{1}{2},k}\\
D_2 &= \epsilon^{(2)}_{j+\frac{1}{2},k}\Delta_\xi Q_{j,k}-\epsilon^{(4)}_{j+\frac{1}{2},k}\nabla_\xi\Delta_\xi\nabla_\xi Q_{j,k}\\
\epsilon^{(2)}_{j,k} &= \kappa_2\Delta t\max(\Upsilon_{j+1,k},\Upsilon_{j,k},\Upsilon_{j-1,k})\\
\epsilon^{(4)}_{j,k} &= \max(0,\kappa_4\Delta t-\epsilon^{(2)}_{j,k})\\
\Upsilon_{j,k} &= \frac{|p_{j+1,k}-2p_{j,k}+p_{j-1,k}|}{|p_{j+1,k}+2p_{j,k}+p_{j-1,k}|}
\end{aligned}$$

where δ_ξ is a second-order centered difference operator, Δ_ξ and ∇_ξ are first-order forward and backward difference operators, U is a contravariant velocity component, and κ_2 and κ_4 are constants. Typical values of κ_2 and κ_4 are 1.0 and 0.01 respectively. The term $\Upsilon_{j,k}$ is a pressure switch to control the use of first-order dissipation near shock waves. The shock capturing capabilities of the scheme can be further improved through the use of more complex flux limiters.[6]

The matrix $|A|$ is given by

$$|A| = T_\xi |\Lambda|_\xi T_\xi^{-1} \tag{10}$$

where the columns of T_ξ are the right eigenvectors of A, the flux Jacobian, and

$$|\Lambda|_\xi = \begin{bmatrix} |U| & 0 & 0 & 0 \\ 0 & |U| & 0 & 0 \\ 0 & 0 & |U + c\psi| & 0 \\ 0 & 0 & 0 & |U - c\psi| \end{bmatrix} \tag{11}$$

with $\psi = \sqrt{\xi_x^2 + \xi_y^2}$. The terms in the η direction are analogous.

Near stagnation points and sonic points, some of the eigenvalues of A approach zero. In order to avoid the problems this may introduce, the elements of $|\Lambda|_\xi$ can be modified as follows:

$$\begin{aligned} \tilde{\lambda}_1, \tilde{\lambda}_2 &= \max(\lambda_{1,2}, V_l \sigma) \\ \tilde{\lambda}_3 &= \max(\lambda_3, V_n \sigma) \\ \tilde{\lambda}_4 &= \max(\lambda_4, V_n \sigma) \end{aligned} \tag{12}$$

where σ represents the spectral radius of the flux Jacobian. The constants V_l and V_n can be set to zero for subsonic flows, but finite values are needed for transonic flows. Commonly used values are $V_l = 0.025$, $V_n = 0.25$. The scheme has been implemented using an efficient matrix-vector multiply technique as presented in Ref. 6.

CUSP Dissipation Scheme

The CUSP[8,9] scheme is formulated by a combination of differences of the state and flux vectors. We consider the ECUSP version only, and refer to it as the CUSP scheme for the remainder of the paper.

The first-order CUSP scheme for the ξ coordinate direction is given by

$$\begin{aligned} d_{j+\frac{1}{2},k} &= \frac{1}{2} J^{-1}_{j+\frac{1}{2},k} \alpha^\star_{j+\frac{1}{2},k} c \left(Q_{j+1,k} - Q_{j,k} \right) \\ &\quad + \frac{1}{2} J^{-1}_{j+\frac{1}{2},k} \beta_{j+\frac{1}{2}} \Delta E_{j+\frac{1}{2},k} \end{aligned} \tag{13}$$

where

$$\begin{aligned} \Delta E_{j+\frac{1}{2},k} &= \xi_{x_{j+\frac{1}{2},k}} \left(E_{j+1,k} - E_{j,k} \right) \\ &\quad + \xi_{y_{j+\frac{1}{2},k}} \left(F_{j+1,k} - F_{j,k} \right) \end{aligned}$$

The vectors E and F are the flux vectors written in Cartesian coordinates. The factor c (local speed of sound) is included so that $\alpha^\star$ is dimensionless. The parameters $\alpha^\star$ and β are given by

$$\alpha^\star c = \alpha c - \beta \overline{U} \tag{14}$$

$$\beta = \begin{cases} \max\left(0, \frac{\overline{U} + \lambda^-}{\overline{U} - \lambda^-}\right) & \text{if } 0 \le M \le 1 \\ -\max\left(0, \frac{\overline{U} + \lambda^+}{\overline{U} - \lambda^+}\right) & \text{if } -1 \le M < 0 \\ \text{sign(M)} & \text{if } |M| > 1 \end{cases} \tag{15}$$

where

$$\lambda^\pm = U \pm c\sqrt{\xi_x^2 + \xi_y^2}$$

and α is chosen to equal $|\overline{U}|/c$. Jameson[9] notes that near stagnation points it is sometimes necessary to modify α such that $\alpha = \frac{1}{2}\left(\alpha_0 + \frac{M^2}{\alpha_0}\right)$ when $|M|$ is smaller than α_0. This modification was not required for the viscous test cases presented in this study. The symbol $\overline{U}$ is the arithmetic mean contravariant velocity, while the eigenvalues $\lambda^\pm$ are determined at the Roe state. The choice of the parameters $\alpha^\star$ and β indicates that for Mach numbers below 0.5, the CUSP scheme is a scalar scheme with a scaling based on the contravariant velocity component. For supersonic flows the CUSP scheme becomes an upwind scheme. The CUSP scheme is not total-variation-diminishing and does not guarantee an oscillation-free solution. However, it has been formulated to produce single-point shocks for inviscid flows.

To construct a higher-order CUSP scheme, limiters are added which activate near flow discontinuities. Jameson[8] introduced the following limiter function

$$R(u, v) = 1 - \left| \frac{u - v}{|u| + |v|} \right|^q \tag{16}$$

where we have used $q = 2$. A higher order CUSP scheme is obtained by defining the limited average,

$$L(u, v) = \frac{1}{2} R(u, v)\,(u + v) \tag{17}$$

and then constructing the appropriate left and right states for each variable,

$$\begin{aligned} Q_L^{(n)} &= Q_j^{(n)} + \frac{1}{2} L\left(\Delta Q^{(n)}_{j+\frac{3}{2},k}, \Delta Q^{(n)}_{j-\frac{1}{2},k}\right) \\ Q_R^{(n)} &= Q_{j+1}^{(n)} - \frac{1}{2} L\left(\Delta Q^{(n)}_{j+\frac{3}{2},k}, \Delta Q^{(n)}_{j-\frac{1}{2},k}\right) \end{aligned} \tag{18}$$

where the superscript n represents the nth element of the state vector. Consequently, the dissipative flux becomes

$$\begin{aligned} d_{j+\frac{1}{2},k} &= \frac{1}{2} J^{-1}_{j+\frac{1}{2},k} \alpha^\star_{j+\frac{1}{2},k} \left(Q_{R,k} - Q_{L,k} \right) \\ &\quad + \frac{1}{2} J^{-1}_{j+\frac{1}{2},k} \beta_{j+\frac{1}{2}} \Delta E(Q_{R,L_{j+\frac{1}{2},k}}) \end{aligned} \tag{19}$$

where

$$\Delta E(Q_{R,L_{j+\frac{1}{2},k}}) = \xi_{x_{j+\frac{1}{2},k}}(E(Q_{R,k}) - E(Q_{L,k})) + \xi_{y_{j+\frac{1}{2},k}}(F(Q_{R,k}) - F(Q_{L,k}))$$

Analogous terms appear in the η direction.

A modification to the limited average is suggested by Swanson *et al.*[11] where a free parameter is introduced in order to decouple the constant scaling the first-order dissipation from the constant scaling the third-order dissipation. We found that for the test cases presented, the accuracy of the solution was not significantly influenced by this parameter.

Near a flow discontinuity, u and v in Eq. 16 have opposite signs and therefore $R(u,v) \to 0$. A problem with this limiter function is that it is insensitive to the relative magnitudes of u and v. In near constant regions of the flow field, small fluctuations in u and v can trigger the limiter randomly, which may stall the convergence of the solution. One way to overcome this difficulty is to freeze the limiter once the convergence rate stalls. A better approach is suggested by Jameson,[8] who follows the work of Venkatakrishnan.[17] The limiter function is modified as follows,

$$R(u,v) = 1 - \left| \frac{u-v}{\max\left(|u| + |v|, (\varepsilon\Delta x)^{\frac{3}{2}}\right)} \right|^q \tag{20}$$

where

$$\Delta x = \sqrt{x_\xi^2 + x_\eta^2}$$

This 'soft limiter' introduces a threshold below which first-order dissipation is not activated, and therefore, triggering of the limiter for small extrema does not occur. For inappropriate values of ε, the resulting threshold may be too high, and consequently, visible oscillations may develop around discontinuities. Venkatakrishnan[17] suggests values for ε between 1.0 and 5.0. We use $\varepsilon = 5.0$ and refer to this limiter as the V limiter.

We also modified Eq. 16 to create a new limiter which is shown below,

$$R(u,v) = 1 - \left| \frac{u-v}{|u| + |v| + \frac{\varepsilon}{|u|+|v|}} \right|^q \tag{21}$$

In this case, the parameter ε controls the activation of the limiter. For transonic flows, appropriate values for ε are between 10^{-2} to 10^{-4}. We use $\varepsilon = 10^{-3}$ and refer to this limiter as the Z limiter. Note that this limiter requires less expense than the V limiter.

The use of the limiters defined by Eqs. 16, 20, and 21 adds considerable computational expense to the algorithm. The limiter value has to be computed for each state variable at each node for each direction (i.e., eight evaluations of the limiter function) compared to just two evaluations per node of the pressure switch function. Further, the inversion of the left-hand-side of the implicit algorithm becomes less efficient due to the fact that the limiter may apply different values to each conservation equation. To increase the efficiency of the algorithm we also consider the use of the pressure variable in the Z limiter, with the same limiting applied to each conservation equation. We refer to this limiter as the ZP limiter. Its computational cost is equivalent to that of the pressure switch.

On the left-hand-side of the implicit approximately-factored algorithm, we use the diagonal form. The eigenvalues associated with the CUSP scheme, and the appropriate limiter values are added to the diagonal entries.

Locally Preconditioned CUSP Scheme

For low Mach number flow, the CUSP scheme reduces to scalar dissipation with scaling proportional to the contravariant velocity component. Swanson *et al.*[11] note that with this scaling, CUSP dissipation is well suited for low Mach number flow, since a similar scaling is used by the preconditioned JST scheme, provided that the dissipation is augmented by the preconditioning matrix.

To demonstrate the necessity of augmenting the CUSP dissipation vector by the preconditioning matrix Γ, consider the following analysis. We use the 1-D Euler equations to express the order of magnitude of the elements in the Γ matrix, state vector, and flux vector in terms of ϵ. Recall that effective low Mach number preconditioning is obtained with $\epsilon = M^2$, which is given in Eq. 7.

For low Mach number flow, the changes in the state vector (q) scale with ϵ as follows,

$$\Delta q = \begin{bmatrix} \Delta\rho \\ \Delta\rho u \\ \Delta e \end{bmatrix} = \begin{bmatrix} \mathcal{O}(\epsilon) \\ \mathcal{O}\left(\epsilon^{\frac{1}{2}}\right) \\ \mathcal{O}(\epsilon) \end{bmatrix} \tag{22}$$

The order of magnitude for a scalar scaling proportional to $\overline{u}$, as used by the CUSP scheme for low Mach numbers, is $\mathcal{O}(\epsilon^{\frac{1}{2}})$. Therefore, first-order CUSP dissipation can be expressed in terms of the order of ϵ as follows,

$$\overline{u}\Delta q = \begin{bmatrix} \mathcal{O}\left(\epsilon^{\frac{3}{2}}\right) \\ \mathcal{O}(\epsilon) \\ \mathcal{O}\left(\epsilon^{\frac{3}{2}}\right) \end{bmatrix} \tag{23}$$

The order of the dissipation vector should be the same as the flux vector. The order of magnitude for the flux vector is

$$\Delta f = \begin{bmatrix} \Delta\rho u \\ \Delta(\rho u^2 + p) \\ \Delta u(e+p) \end{bmatrix} = \begin{bmatrix} \mathcal{O}\left(\epsilon^{\frac{1}{2}}\right) \\ \mathcal{O}(\epsilon) \\ \mathcal{O}\left(\epsilon^{\frac{1}{2}}\right) \end{bmatrix} \tag{24}$$

Comparing Eq. 24 with Eq. 23 reveals that the mass and energy conservation equations may have insufficient dissipation. This could cause poor convergence characteristics.

In order to make the order of the dissipation vector consistent with the flux vector, consider the Γ matrix whose entries in terms of the order of ϵ are

$$\Gamma = \begin{bmatrix} \mathcal{O}(1) & \mathcal{O}\left(\epsilon^{-\frac{1}{2}}\right) & \mathcal{O}\left(\epsilon^{-1}\right) \\ \mathcal{O}(\epsilon) & \mathcal{O}(1) & \mathcal{O}\left(\epsilon^{-\frac{1}{2}}\right) \\ \mathcal{O}(1) & \mathcal{O}\left(\epsilon^{-\frac{1}{2}}\right) & \mathcal{O}\left(\epsilon^{-1}\right) \end{bmatrix} \tag{25}$$

Then the product $\Gamma\Delta q$ becomes

$$\Gamma\Delta q = \begin{bmatrix} \mathcal{O}(1) \\ \mathcal{O}\left(\epsilon^{\frac{1}{2}}\right) \\ \mathcal{O}(1) \end{bmatrix} \tag{26}$$

Now, if the dissipation vector is augmented by the preconditioning matrix in the following manner,

$$\overline{u}\Gamma\Delta q = \begin{bmatrix} \mathcal{O}\left(\epsilon^{\frac{1}{2}}\right) \\ \mathcal{O}(\epsilon) \\ \mathcal{O}\left(\epsilon^{\frac{1}{2}}\right) \end{bmatrix} \tag{27}$$

the order of the dissipation vector is consistent with the order of the flux vector.

Hence, to obtain the preconditioned CUSP scheme for flow with freestream Mach number below 0.5, modify Eq. 13 as follows

$$d_{j+\frac{1}{2},k} = \frac{1}{2}\alpha^{\star}_{j+\frac{1}{2},k} c\Gamma_{j+\frac{1}{2},k} J^{-1}_{j+\frac{1}{2},k}\left(Q_{j+1,k} - Q_{j,k}\right) \tag{28}$$

where

$$\alpha^{\star} = \frac{\bar{U}}{c}$$

Both V and Z limiters can be used with the scheme; however, the subsonic test case studied did not require these limiters.

To evaluate the preconditioned CUSP scheme, we compare with the preconditioned JST scheme which was studied in Ref. 12. The preconditioned JST scheme is obtained from Eq. 9 as follows,

$$D_1 = 2\sigma_{j+\frac{1}{2},k}\Gamma_{j+\frac{1}{2},k} J^{-1}_{j+\frac{1}{2},k} \tag{29}$$

where

$$\sigma_{j,k} = \frac{1}{2}(1+\epsilon)\left|U_\xi\right| + \frac{1}{2}\sqrt{(\epsilon-1)^2 U_\xi^2 + 4\epsilon\left(\xi_x^2+\xi_y^2\right)c^2}$$

Results and Discussion

In order to evaluate the CUSP numerical dissipation scheme, the following test cases are examined:

1. M_∞=0.16, α=0°, Re=2.88 × 10^6, transition at 0.43 chords on both surfaces, NACA 0012 airfoil.
2. M_∞=0.16, α=6°, Re=2.88×10^6, transition at 0.05 and 0.8 chords on the upper and lower surfaces, respectively; NACA 0012 airfoil.
3. M_∞=0.7, α=3°, Re=9.0 × 10^6, transition at 0.05 chords on both surfaces, NACA 0012 airfoil.
4. M_∞=0.729, α=2.31°, Re=6.5 × 10^6, transition at 0.03 chords on both surfaces, RAE 2822 airfoil.
5. $M_\infty = 0.01, 0.05, 0.1, 0.2, 0.3, 0.4$, $\alpha = 2.0°$, $Re = 2.88 \times 10^6$, transition at 0.05 and 0.25 chords on the upper and lower surfaces, respectively; NACA 0012 airfoil.

Grid	JDIM	KDIM	Body Points	Wake Points	Off-Wall Spacing
A	1057	193	801	129	2.3×10^{-7}
B	529	97	401	65	5.3×10^{-7}
C	265	49	201	33	1.2×10^{-6}
P	279	49	201	40	2×10^{-6}

Table 1 Summary of grids.

Table 1 is a summary of the grids used. All of the grids have a "C" topology. In Table 1 'JDIM' represents the number of points in the streamwise direction, 'KDIM' represents the number of points in the normal direction, 'Body Points' represents the number of points on the body, 'Wake Points' represents the number of points in the wake, and 'Off-Wall Spacing' is the normal spacing to the first grid line off of the surface in chords. The distance to the outer boundary is 12 chords for all grids. For grid A, the leading edge clustering is 0.0001, and the trailing edge clustering is 0.0002. Grid B was generated by removing every second node in both coordinate directions from grid A, and similarly, grid C was generated by removing every second node in both coordinate directions from grid B. Grid P is used to evaluate case 5. We found that the presence of high aspect cells stretched in the normal direction with respect to the flow appeared to cause the preconditioned algorithm to diverge on grid C. Hence grid P was constructed with a less aggressive trailing edge clustering of 0.001, and additional nodes were placed in the wake.

Flux Limiters

Transonic flows require limiters to activate in the region of flow discontinuities, such as shocks, to ensure good convergence rates and to preserve the monotonicity of the solution. For the V, Z, and ZP limiters introduced in Eqs. 20 and 21, a value of ε was selected such that limit cycles are avoided yet reasonably oscillation-free shocks are obtained. A parameter search was performed to find the value of ε for which accuracy, shock capturing, and convergence are optimum.

Dissipation	ε	C_l	C_d	C_{d_p}	C_{d_f}
CUSP Z	1×10^{-2}	-1.2	0.5	3.7	-5.0
CUSP Z	1×10^{-3}	-0.9	1.0	4.9	-5.8
CUSP Z	1×10^{-4}	-1.0	2.4	6.5	-4.6
CUSP ZP	1×10^{-2}	-1.1	0.6	3.9	-5.2
CUSP ZP	1×10^{-3}	-0.7	1.5	5.3	-4.8
CUSP ZP	1×10^{-4}	-0.7	2.6	6.9	-4.6
CUSP V	10.0	-0.8	1.2	5.3	-5.6
CUSP V	5.0	-0.9	1.8	5.9	-4.8
CUSP V	1.0	-0.8	2.8	7.7	-5.4
Matrix	-	-0.8	4.2	7.9	-2.6

Table 2 Sensitivity of solution to ε for Case 3.

Table 2 shows the sensitivity of the aerodynamic coefficients to the parameter ε. The entries give the percent difference in the lift coefficient, C_l, drag coefficient, C_d, the pressure drag component, C_{d_p}, and the friction drag component, C_{d_f}, from the results obtained on grid A. Note that for all limiters, more first-order dissipation is introduced as ε is reduced. Smallest errors in the aerodynamic coefficients were obtained with relatively large values of ε, specifically 10.0 with the V limiter, and 0.01 for the Z and ZP limiters. With these values, the limiters introduce less first-order dissipation, and therefore, greater accuracy is achieved. Values of ε below 1×10^{-4} for the Z limiter and 5.0 for the V limiter yield relatively large errors.

Shock capturing for the same range of ε values as given in Table 2 was examined for the three limiters. Shocks with two interior points were obtained for all values of ε. For the V limiter, values of ε should not exceed 10.0, while for the Z and ZP limiters, the values should be kept below 0.01 in order to obtain oscillation-free shocks. Also, the effect of ε on the convergence rate of the solver was evaluated. Generally, if the convergence rate stalls as the residual passes through the first two orders of magnitude, the limiter is trapped in a limit cycle. For the V limiter, best convergence rates were obtained for values of ε less than 1.0, while for the Z and ZP limiters the convergence rate stalled for values of ε below 1×10^{-4}.

Hence, in terms of accuracy, shock capturing, and convergence rate, the optimal value of ε is 5 for the V limiter and 1×10^{-3} for the Z and ZP limiters. Similar results were observed for other transonic test cases.

Dissipation in Boundary Layers

Next we examine the amount of numerical dissipation introduced in boundary layers, and whether it interferes with the desired balance between convective and viscous fluxes. The streamwise momentum equation is typically most revealing. Fig. 1 shows the x-momentum flux balance for case 1 computed on grid C with the matrix and CUSP schemes. The user selected parameters for matrix dissipation were set to $\kappa_2 = 0$ and $\kappa_4 = 0.01$, with $V_n = V_l = 0$. For CUSP dissipation, the limiters were not activated. The station shown is at $x/c = 0.6$, where the boundary layer thickness is roughly 0.008 chords and the flow is turbulent. There are roughly 25 points across the boundary layer. Ideally, the viscous flux should balance the convective flux with only a minimal contribution from the numerical dissipation. This is well illustrated by both schemes in Fig. 1. Consequently, the solutions obtained by the matrix and CUSP schemes are very similar. Even on the coarser grid C, the drag coefficient was within 1.5% of the drag coefficient computed on grid A for both schemes.

Shock Capturing

Pressure coefficient distributions for case 3 are shown in Fig. 2. Both matrix and CUSP dissipation capture the shock very well as shown in Fig. 2(b). The quality of shock capture for the pressure based ZP limiter is approximately the same as for the Z limiter, but note that the computational efficiency of the algorithm is significantly improved. Swanson *et al.*[11] observed that for transonic viscous flow the HCUSP scheme captured shocks which were too far upstream. Clearly, the present results with ECUSP do not have the same difficulty, and the captured shock locations agree with the matrix scheme. Note that single-point shocks are obtained when using the CUSP scheme for inviscid flows.

Accuracy

Figs. 3 to 5 show the grid convergence of the lift coefficient, C_l, drag coefficient, C_d, the pressure drag component, C_{d_p}, and the friction drag component, C_{d_f}, for cases 2, 3, and 4. The results are plotted vs $1/N$ where N is the total number of grid nodes. These figures show that matrix dissipation is slightly more accurate in predicting the lift coefficient and the friction drag coefficient. The CUSP scheme produces more accurate pressure drag values for the transonic cases. Note that error cancellation between the C_{d_p} and C_{d_f} values may influence the the global C_d error. Results computed with the less expensive ZP limiter are very similar to those obtained using the full Z limiter.

Convergence

The convergence histories for cases 2 and 4 are shown in Fig. 6. The different numerical dissipation schemes have little effect on the convergence rate.

Computational Efficiency

The matrix scheme with the pressure switch requires $15 - 20\%$ more computational effort than the JST scheme, depending on the details of the implementation, primarily as a result of the need to form $|A|$ and the corresponding matrix-vector product. The CUSP scheme with the ZP limiter has a computational cost only $5 - 10\%$ greater than the JST scheme. The cost

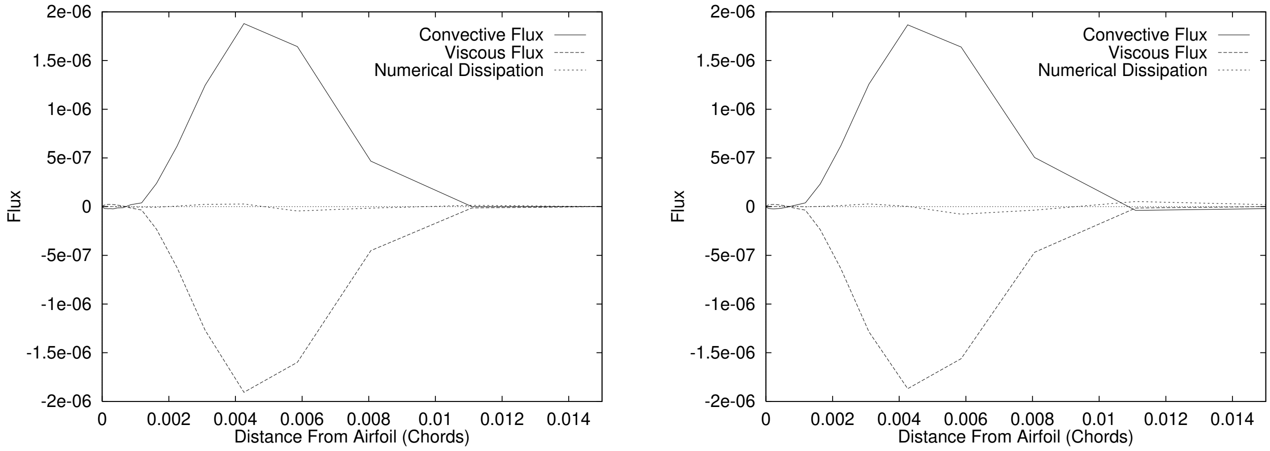

a) Matrix Dissipation

b) CUSP Dissipation

Fig. 1 Flux balance for Case 1 on grid C at 60% chord.

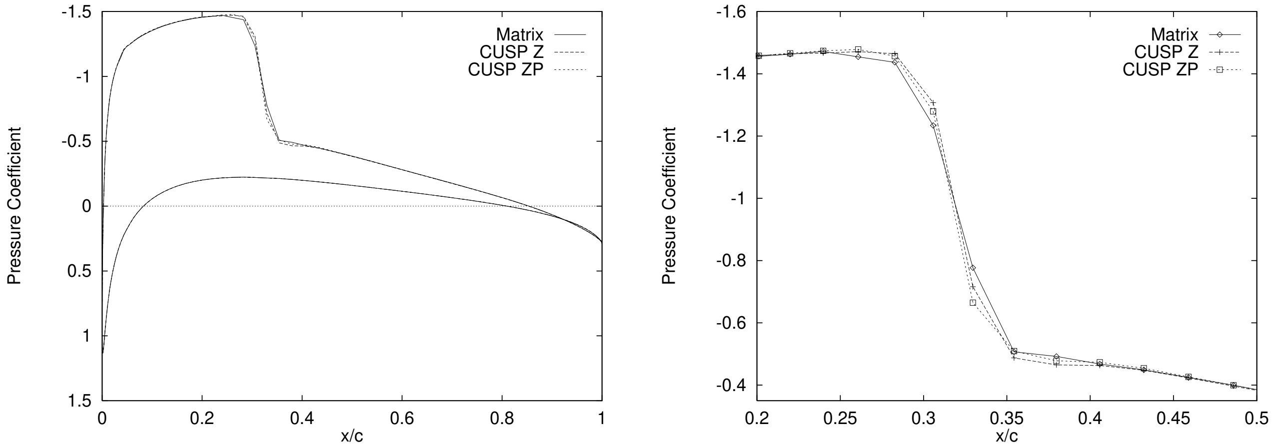

a) C_p

b) Close-up of shock region.

Fig. 2 Computed pressure distributions for case 3.

is associated with the use of the Roe average. With the Z limiter, the CUSP scheme requires about 35% more effort than the JST scheme, and with the V limiter about 40%, which is due to the evaluation of the limiter. Clearly the use of the simple pressure-based limiter provides significant savings.

Local Preconditioning

Results for case 5 are presented in Figure 7(a), which shows the variation of the computed drag with the freestream Mach number for the original CUSP, preconditioned CUSP, and preconditioned JST schemes calculated on grid P. The original CUSP scheme without preconditioning shows dependence on the Mach number for Mach numbers less than 0.15. The preconditioned scalar and CUSP schemes correctly illustrate the lack of dependence of drag on the Mach number for the given Mach number range. Furthermore, the drag obtained with the preconditioned CUSP scheme is lower than that obtained with the preconditioned scalar dissipation. The drag coefficient computed with matrix dissipation on the finest grid A is about 0.00836 for this case. On the coarser grid P, the preconditioned CUSP dissipation is within 1% of this result for the whole Mach number range, while for the preconditioned JST scheme the error is 6%. Hence, although the JST scheme is greatly improved through local preconditioning, the preconditioned CUSP scheme is substantially more accurate.

Fig. 7(b) shows the convergence of drag for the CUSP scheme with and without local preconditioning for the freestream Mach number of 0.05. For the preconditioned algorithm, drag converges within 500 iterations, while without preconditioning, 2500 iterations are required to obtain a converged value.

Although the dissipation coefficient of the JST scheme is smaller than that of the CUSP scheme, the results indicate that the CUSP scheme introduces far less dissipation. This is due to the fact that for grids with cells which are reasonably aligned with the flow, $\alpha^{\star}$ is smaller in the normal direction when compared with the preconditioned spectral radius of the JST scheme, where ϵ is based on the flow Mach number. This is also true for the original CUSP and JST schemes, since the contribution of the spectral radius

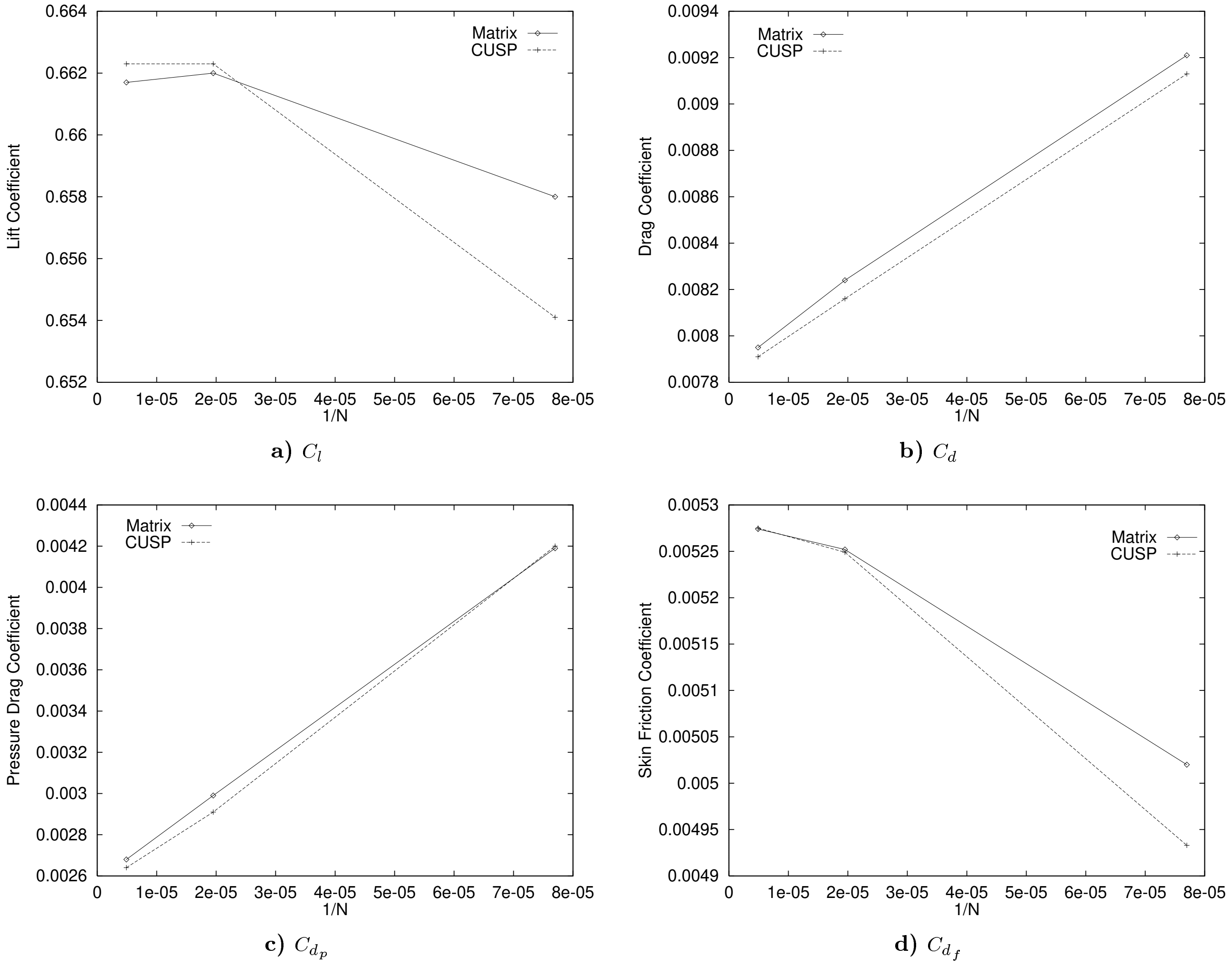

a) C_l b) C_d

c) C_{d_p} d) C_{d_f}

Fig. 3 Grid convergence for case 2.

is large in both ξ and η directions for the JST scheme due to the presence of the speed of sound. With the CUSP scheme, the scaling is based on the local contravariant velocity component.

Concluding Remarks

Our results indicate that the CUSP scheme provides accuracy which is comparable to the matrix numerical dissipation scheme. When used together with the inexpensive ZP limiter based on pressure, the cost of the CUSP scheme is comparable to that of the original JST scheme. Hence the CUSP scheme achieves its goal of providing accuracy comparable to a high-resolution scheme, at least for aerodynamic computations, at a cost similar to the JST scheme.

Acknowledgments

The first author was supported by an OGS grant of the Government of Ontario. This research was supported by AEA Technology–Advanced Scientific Computing Ltd., and the Natural Sciences and Engineering Research Council of Canada.

References

[1]Jameson, A., Schmidt, W., and Turkel, E., "Numerical Solutions of the Euler Equations by Finite Volume Methods Using Runge-Kutta Time Stepping," AIAA Paper 81–1259, June 1981.

[2]Allmaras, S. R., "Contamination of Laminar Boundary Layers by Artificial Dissipation in Navier-Stokes Solutions," *Numerical Methods for Fluid Dynamics*, edited by M. J. Baines and K. W. Morton, Claredon Press, Oxford, 1993.

[3]Frew, K. and Zingg, D. W., "On Artificial Dissipation Models for Viscous Airfoil Computations," AIAA Paper 96–1970, June 1996.

[4]Roe, P. L., "Approximate Riemann Solvers, Parameter Vectors, and Difference Schemes," *J. Comp. Phys.*, Vol. 43, 1981, pp. 357–372.

[5]Van Leer, B., "Flux Vector Splitting for the Euler Equations," *Proceedings of the 8th International Conference on Numerical Methods in Fluid Dynamics*, edited by E. Krause, No. 170, 1982, pp. 507–512.

[6]Swanson, R. C. and Turkel, E., "On Central-Difference and Upwind Schemes," *J. Comp. Phys.*, Vol. 101, 1992, pp. 292–306.

[7]Harten, A., "High Resolution Schemes for Hyperbolic Conservation Laws," *J. Comp. Phys.*, Vol. 49, 1983, pp. 357–393.

[8]Jameson, A., "Analysis and Design of Numerical Schemes for Gas Dynamics I: Artificial Diffusion, Upwind Biasing, Limiters and their Effect on Accuracy and Multigrid Convergence," *Inter. J. Comp. Fluid Dynamics*, Vol. 4, 1995, pp. 171–218.

[9]Jameson, A., "Analysis and Design of Numerical Schemes for Gas Dynamics II: Artificial Diffusion and Discrete Shock

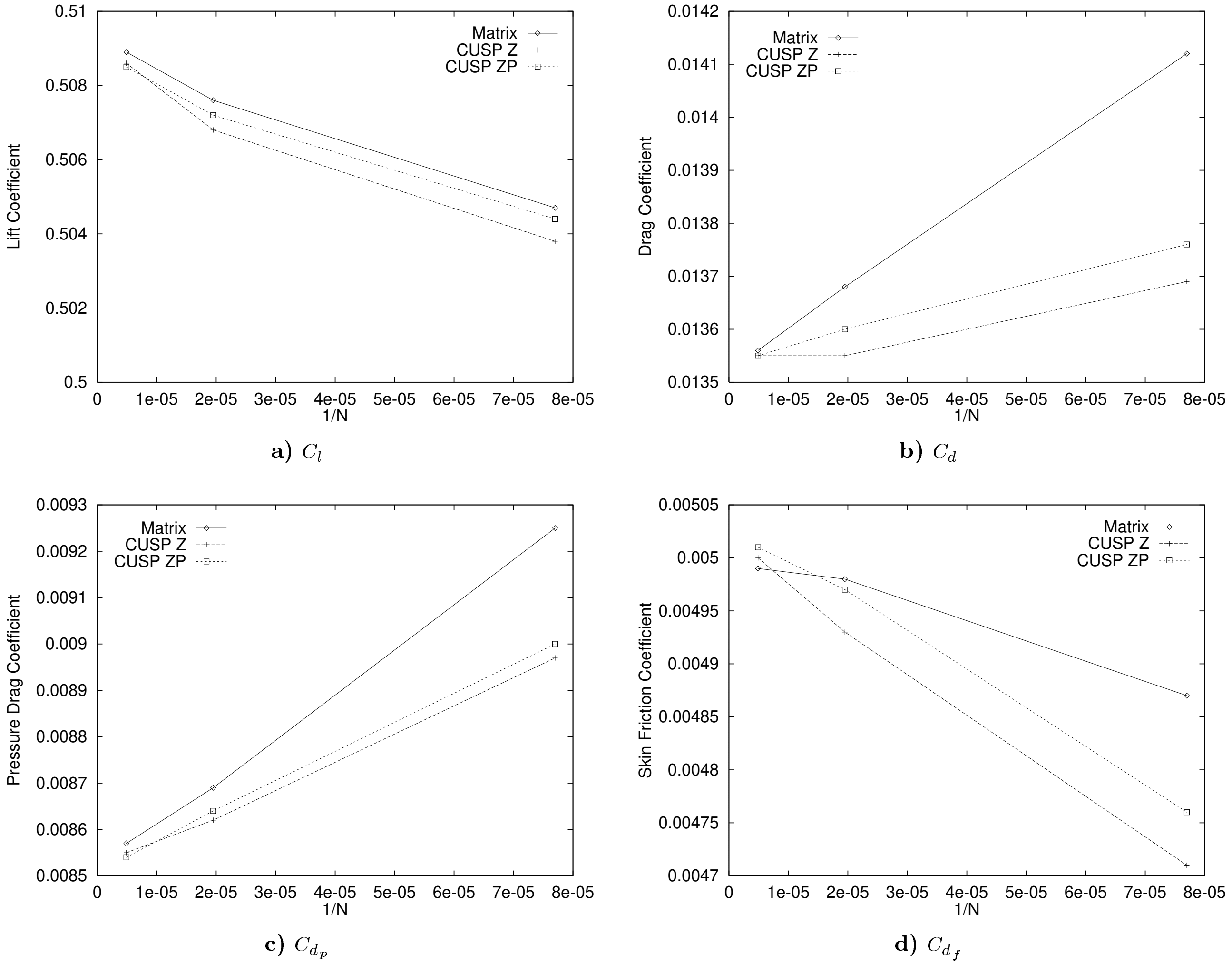

a) C_l **b)** C_d

c) C_{d_p} **d)** C_{d_f}

Fig. 4 Grid convergence for case 3.

Structure," *Inter. J. Comp. Fluid Dynamics*, Vol. 5, 1995, pp. 1–38.

[10] Tatsumi, S., Martinelli, L., and Jameson, A., "A New High Resolution Scheme for Compressible Viscous Flow with Shocks," AIAA Paper 95–0466, Jan. 1995.

[11] Swanson, R. C., Radespiel, R., and Turkel, E., "Comparison of Several Dissipation Algorithms for Central Difference Schemes," AIAA Paper 97–1945, June 1997.

[12] Unrau, D. and Zingg, D. W., "Viscous Airfoil Computations Using Local Preconditioning," AIAA Paper 96–2088, June 1996.

[13] Weiss, J. M. and Smith, W. A., "Preconditioning Applied to Variable and Constant Density Flows," *AIAA Journal*, Vol. 33, No. 11, 1997, pp. 2050–2057.

[14] Pulliam, T. H., "Efficient Solution Methods for the Navier-Stokes Equations," Tech. rep., Lecture Notes for the Von Karman Institute for Fluid Dynamics Lecture Series, Brussels, Jan. 1986.

[15] Choi, Y. H. and Merkle, C. L., "The Application of Preconditioning in Viscous Flows," *J. Comp. Phys.*, Vol. 105, 1993, pp. 207–233.

[16] Turkel, E., "Preconditioned Methods for Solving the Incompressible and Low Speed Compressible Equations," *J. Comp. Phys.*, Vol. 72, 1987, pp. 277–298.

[17] Venkatakrishnan, V., "Convergence to Steady State Solutions of the Euler Equations on Unstructured Grids with Limiters," *J. Comp. Phys.*, Vol. 118, 1995, pp. 120–130.

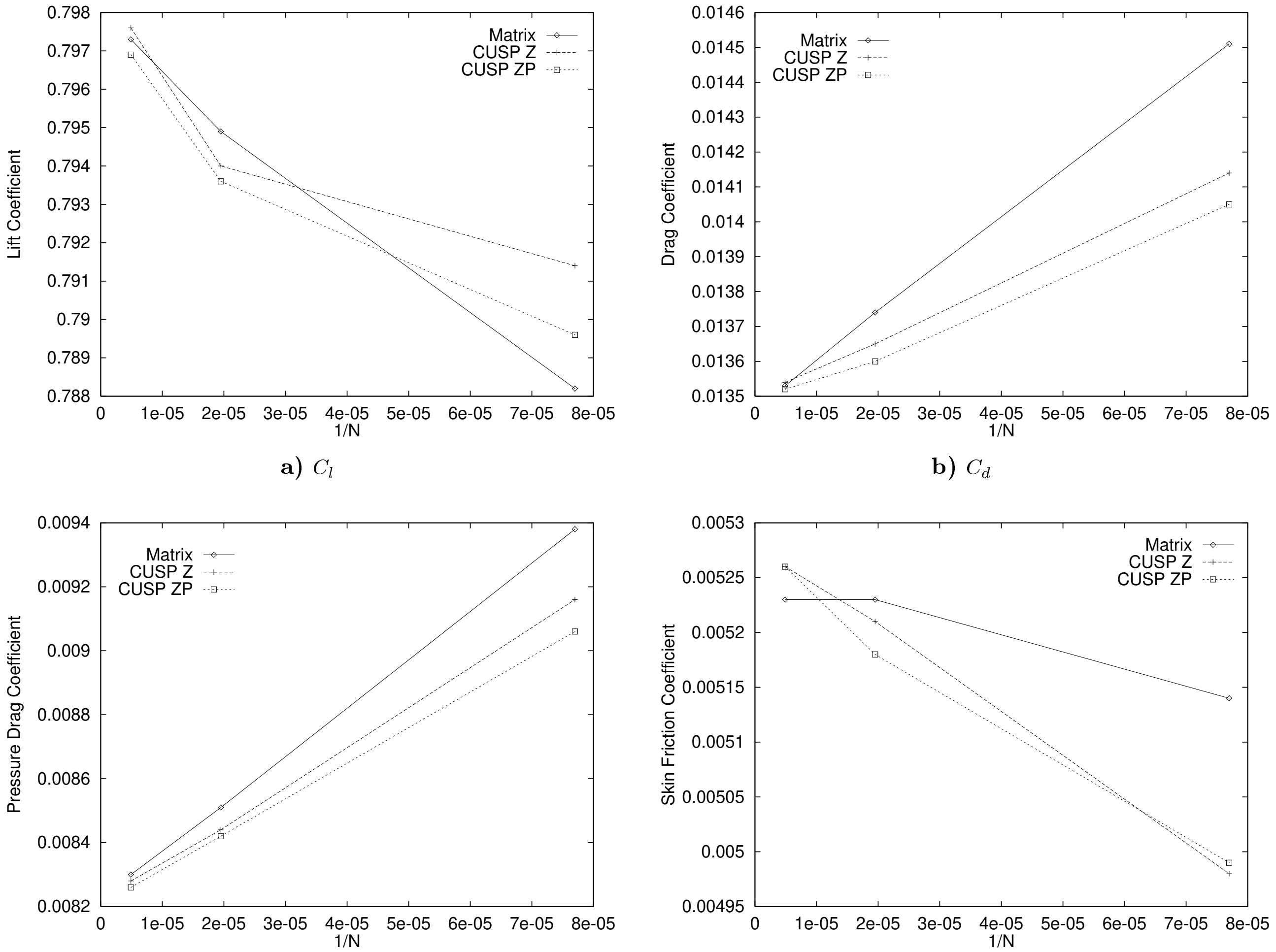

a) C_l **b)** C_d

c) C_{d_p} **d)** C_{d_f}

Fig. 5 Grid convergence for case 4.

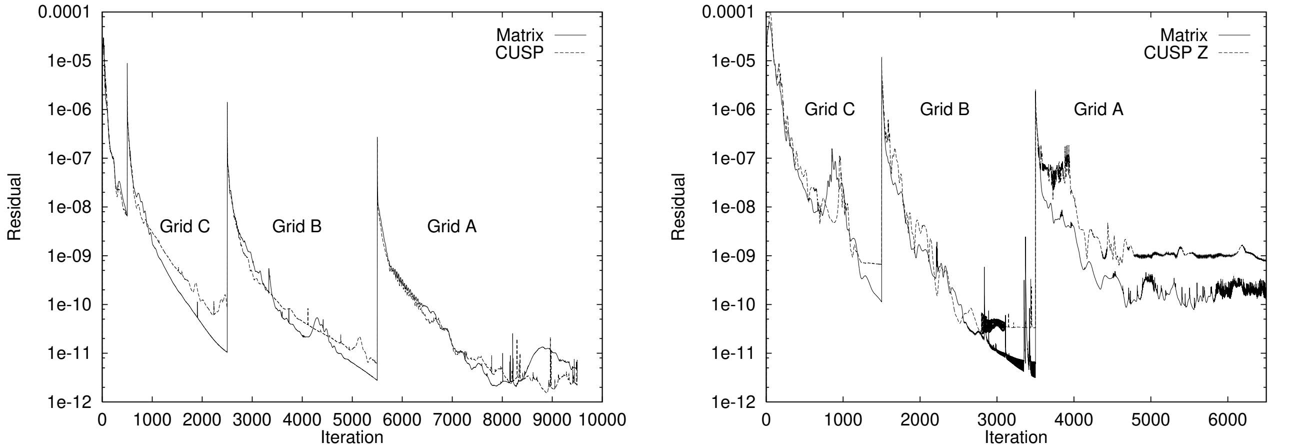

a) Case 2 **b)** Case 4

Fig. 6 Residual convergence history.

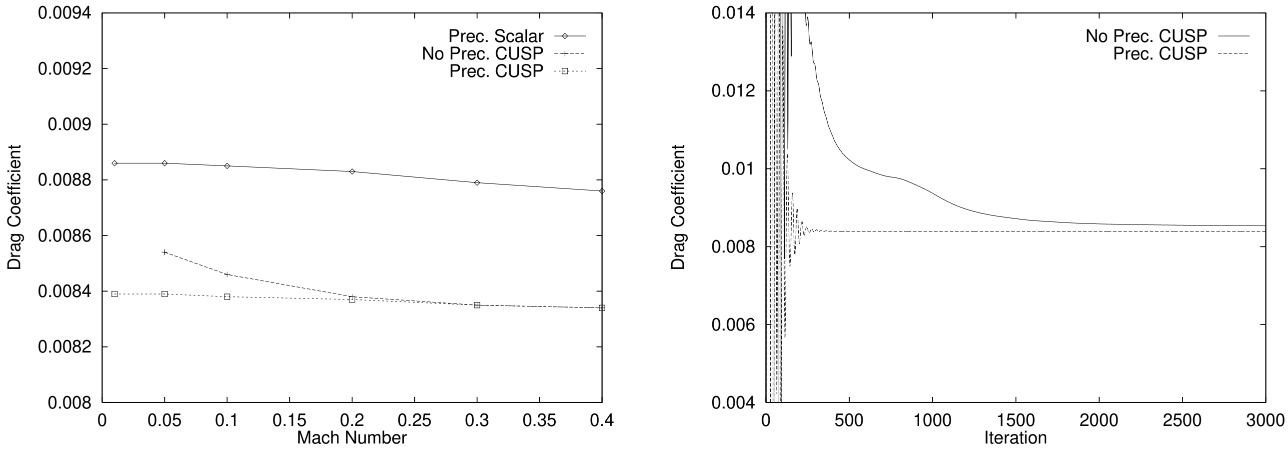

a) Computed drag coefficient.

b) Drag convergence at $M_\infty = 0.05$.

Fig. 7 Preconditioning results for case 5.